ADVANCES IN ATMOSPHERIC SCIENCES, VOL. 20, NO. 5, 2003, PP. 755–766

The Change of North China Climate in Transient Simulations Using the IPCC SRES A2 and B2 Scenarios with a Coupled Atmosphere-Ocean General Circulation Model

BUHE Cholaw*[1] (布和朝鲁), Ulrich CUBASCH[2], LIN Yonghui[3] (林永辉), and JI Liren[1] (纪立人)

[1] *LASG, Institute of Atmospheric Physics, Chinese Academy of Sciences, Beijing* 100029

[2] *Meteorologisches Institut der Freien Universitaet Berlin, Care-Heinrich-Becker Weg 6–10, 12165*

[3] *Institute of Severe Weather, Chinese Academy of Meteorological Sciences, Beijing* 100081

(Received 26 September 2002; revised 12 February 2003)

ABSTRACT

This paper applies the newest emission scenarios of the sulfur and greenhouse gases, namely IPCC SRES A2 and B2 scenarios, to investigate the change of the North China climate with an atmosphere-ocean coupled general circulation model. In the last three decades of the 21st century, the global warming enlarges the land-sea thermal contrast, and hence, causes the East Asian summer (winter) monsoon circulation to be strengthened (weakened). The rainfall seasonality strengthens and the summer precipitation increases significantly in North China. It is suggested that the East Asian rainy area would expand northward to North China in the last three decades of the 21st century. In addition, the North China precipitation would increase significantly in September. In July, August, and September, the interannual variability of the precipitation enlarges evidently over North China, implying a risk of flooding in the future.

Key words: North China, Climate change, Seasonality, IPCC SRES A2 and B2 scenarios

1. Introduction

The East Asian monsoon (EAM) rainfall is concentrated in the late spring and summer and mainly persists over South China and the Yangtze River valley in different but consecutive months. North China is affected by EAM circulation as well, and hence the peak of the rainfall occurs also in summer even though the amount is small. So, from late spring to summer, the EAM rain band seems to persist over an area in one stage and then to progress northward and finally arrive in North China (Tao and Chen, 1987).

The interannual and interdecadal variabilities of the East Asian climate have been extensively studied (Yasunari, 1991; Lau, 1992; Ji et al., 1997; Chen and Graf, 2000; Bueh and Ji, 1999). However, the research of its change under global warming conditions is relatively limited. Wang and Ye (1993) and Nitta and Hu (1996) found from observational data a pronounced warming trend in North China. With observational data and model simulations, Hulme et al. (1994) proposed that the global warming would have significant impacts on East Asian climate as well as its variations. Hu et al. (2000) found in a transient greenhouse warming integration with a CGCM (coupled general circulation model) that increases of greenhouse gas concentrations reduces the land-sea contrast and, thus, weakens the East Asian winter monsoon. However, so far the impact of the global warming on the annual cycle of East Asian Climate, especially the North China climate, has not been studied.

North China covers the semi-arid and semi-humid regions as well as their transition area, which is the transition zone of diverse biomes. The ecological system in North China, therefore, is very sensitive to climate change and anthropogenic influence. In the last ten years, drought has prevailed here, and hence, its climate variability and change attract more of a concern. In this work, we use the newest emission scenarios, namely the IPCC SRES A2 and B2 scenarios, to investigate the change of the North China climate and its variability.

*E-mail: bueh@lasg.iap.ac.cn

The IPCC Special Report on Emission Scenarios (SRES) described a new set of approved emission scenarios, which are to update and replace the well-known IS92 scenarios (IPCC, 2001). Four different narrative storylines were developed to consistently describe the relationships between the forces driving emissions and their evolutions. 40 SRES scenarios chosen cover a wide range of the main demographic, economic, and technological driving forces of future greenhouse gases and sulfur emissions. Each scenario illustrates a specific quantification of one of the four storylines. Then, four marker scenarios (A1, A2, B1, and B2) were chosen from the four scenarios groups, consistent with the four storylines. The choice of the marker scenario was based on which of the initial quantifications best represented the particular storylines and the features of specific models. Specifically, the A1 scenario assumes a global cooperation and a rapid adaptation of new technologies with a stabilization of the population; the A2 scenario represents a regionally limited cooperation and a slower adaptation of new technologies with an unstabilized population growth; the B1 scenario assumes a global ecological development with a stabilization of the population; and the B2 scenario reflects a regionally limited ecological development. In this study, we select the A2 and B2 scenarios from the four scenarios, since they seem realistically representative of the future emissions.

The purpose of this study is to identify changes of North China climate using the IPCC SRES A2 and B2 scenarios. In section 2, we describe the model used here and the experiment design. The validation of the model for representing the East Asian Climate is given in section 3. The changes of the North China climate and its variability are discussed in section 4. The final section will be a summary and discussion.

2. Model, Experiment, and data

The model used in this work is the ECHAM4/OPYC3 CGCM. The atmospheric component ECHAM4 employs a 19-level hybrid sigma-pressure coordinate system, which extends vertically up to the pressure level of 10 hPa. The prognostic variables are represented by spherical harmonics with triangular truncation at wavenumber 42 (T42, 128×64 grid points on the Gaussian grid). The land surface model comprises the budgets of heat and water, the snow pack over land, and the heat budget of land ice. For details of the ECHAM4, such as the physical parameterization and climate statistics, readers may refer to Roeckner et al. (1996). The OGCM component (OPYC3) developed by Oberhuber (1993) consists of three submodels of the interior ocean, the surface mixed layer, and the sea ice. There are 10 interior vertical layers below the surface mixed layer. Fluxes of heat and fresh water are flux-adjusted annually, while fluxes of momentum are unconstrained. This coupled model has been employed in the project SIDDACLICH (Simulation, Diagnosis, and Detection of the Anthropogenic Climate Change) and its coupling strategy and technology are described in Cubasch et al. (2000). Other details of this model are also found in Bacher et al. (1998).

The model calculates basic aspects of the tropospheric sulfur cycle, such as transport and deposition, and partly also the chemistry (Feichter et al., 1997). Dimethyl-sulfide (DMS), gaseous sulfur dioxide (SO_2), and sulphate aerosol (SO_4^{2-}) are used as prognostic variables. It is important to note that biogenic emission from oceans, soils, and plants are assumed to occur as DMS, while noneruptive volcanic emissions, the burning of biomass, and the combustion of fossil fuel are assumed to take place as SO_2. Transport and diffusion of the sulfur species are treated as for water vapor. A deposition velocity, dependent on the species and on the state of the surface, is used to calculate dry deposition. Wet deposition is parameterized by means of the local precipitation formation rate. During daytime, DMS and SO_2 are oxidized by hydroxyl radicals (OH^-), whereas during the night, DMS reacts with nitrate radicals (NO_3^-). In the aqueous phase, SO_2 is oxidized by ozone (O_3) and hydrogen peroxide (H_2O_2). These species are not calculated in ECHAM4, but rather prescribed as monthly mean 3-dimensional fields, according to estimates by a chemistry model coupled to ECHAM4 (Roelofs and Lelieveld, 1995). In any case, the final product of the oxidation of SO_2 is sulfate aerosol, which interacts radiatively with the atmospheric model through direct and indirect effects. In all simulations of this work, only anthropogenic sources are taken into account, and the biogenic and volcanic sulfur emissions are neglected. From 1990 to

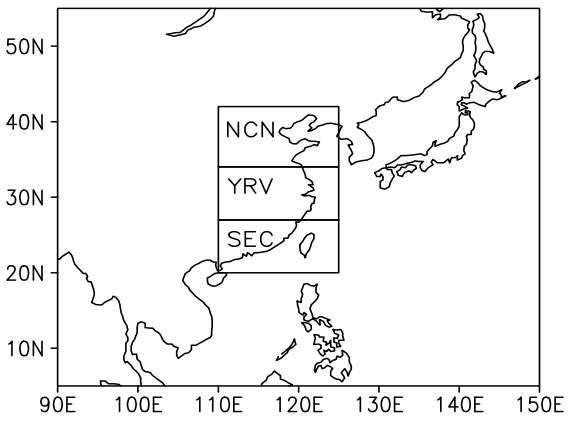

Fig. 1. The geographical locations of the regions under study: the southeastern coastal area (SEC), the Yangtze River valley (YRV), and North China (NCN).

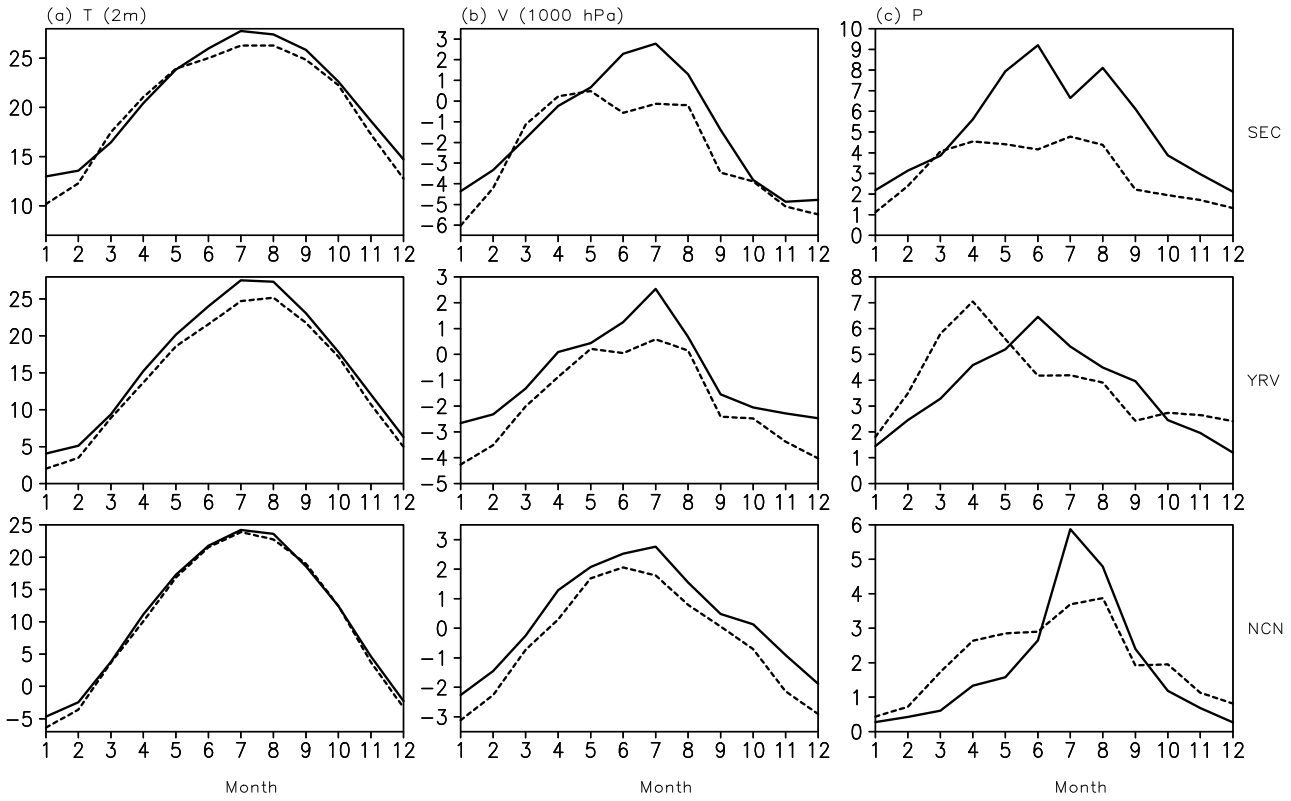

Fig. 2. (a)Annual cycles of 2-m (or surface) air temperatures (°C) for SEC, YRV, and NCN. The solid lines stand for the surface air temperature from CRU data, and the dashed lines for the 2-m temperatures of the simulations. (b) The same as (a), but for the 1000-hPa meridional wind ($m\,s^{-1}$), where the dashed lines represent NCEP reanalysis data. (c) The same as (a), but for the precipitation ($mm\,d^{-1}$).

2100, the emissions are given every ten years with linear interpolation (Nakicenovic et al., 2000).

A 30-year simulation (1961–1990) of the coupled model performed and described by Roeckner et al. (1999), is used here to represent the coupled model present-day climate. In the simulation, apart from the greenhouse gases, direct radiative and indirect (i.e., through cloud albedo) effect of sulfate aerosol are taken into account in a parameterized manner, and the tropospheric ozone distribution is allowed to change as a result of prescribed anthropogenic emissions of precursor gases O_3,H_2O_2,OH^-, and NO_3^-. According to this, this simulation experiment is called "GSDIO" experiment in their work. We will use this name here as well. Only the anthropogenic part of the sulfur emissions is taken into account and prescribed every ten years according to the observation. For the details, readers may refer to Roeckner et al. (1999).

With the ECHAM4/OPYC3 CGCM, two time-dependant forcing experiments according to the A2 and B2 scenarios with prescribed concentration of greenhouse gases and halocarbons and emissions of sulfur have been performed for the period 1990-2100.

In both present-day and future climate simulations, the concentrations of various gases have been prescribed as a function of time: the greenhouse gases CO_2, CH_4, N_2O, and several industrial gases such as chlorofluorocarbons (CFC-11, 12, 113, 114, 115), hydro chlorofluorocarbons (HCFC-22, 123, 141b), hydrochlorocarbons (HFC-125, 134a, 152a), carbon tetrachloride (CCl_4), and methylchloro-form (CH_3CCl_3). For the present-day (future) climate simulations, the annual mean concentrations of all greenhouse gases have been prescribed according to the observational data (IPCC SRES A2 and B2 scenarios).

Apart from these data, we also applied the monthly mean precipitation and surface temperature data (1961–1990) of the Climate Research Unit (CRU, New et al., 2000) and the monthly mean 1000-hPa wind of the National Center for Environmental Prediction (NCEP) reanalysis data (1961–1990) (Kalnay et al., 1996) to validate the simulated ones for the present-

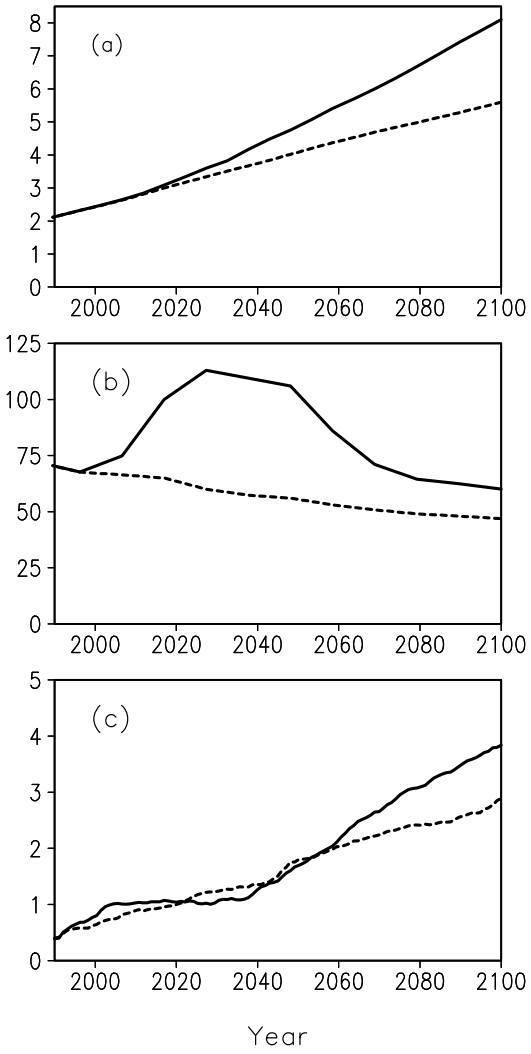

Fig. 3. Temporal evolutions of the global mean (a) radiative forcing of all greenhouse gases (W m^{-2}, annual mean), (b) sulfur emissions (Tg S yr^{-1}, 10-year mean), and (c) 2-m temperature anomalies (°C, 5-year running mean) relative to the present-day simulation. The solid and dashed lines are for the IPCC SRES A2 and B2 scenarios, respectively.

day climate.

3. Validation

The East Asian precipitation during the summer monsoon period is influenced by three distinct but interactive systems, i.e., tropical monsoon that mainly consists of the Southerly flow over the Bay of Bengal and South China Sea, the western Pacific subtropical high (WPSH), and the mid latitude baroclinic disturbances. In particular, the position and march of the WPSH have a crucial effect on that of the East Asian rain band (Chang et al., 2000). Its inadequate representation in the model causes a poor simulation of the East Asian precipitation. To validate how well the model captured the feature of East Asian climate (present-day), we select three key regions to compare their simulated climate with the observational and reanalysis data. The three regions are the southeastern coastal area (SEC, 20°–27°N, 110°–125°E), the Yangtze River valley (YRV, 27°–34°N, 110°–125°E) and North China (NCN, 34°–42°N, 110°–125°E), respectively. Of course, our focus is to validate the simulated climate of North China in comparison with that of the SEC and YRV. In fact, the area (27°–34°N, 110°–125°E) covers the Huaihe River valley as well, but it is always named as the Yangtze River valley (e.g., Chang et al., 2000) and this would not distort the results of this study about the climate change in North China. The geographical locations of the three key regions are displayed in Fig. 1.

Annual cycles of the area-mean 2-m temperatures over the SEC, YRV, and NCN are displayed in Fig. 2a. The annual cycles of the temperature for these regions are well simulated in the present-day climate simulation. However, for the SEC and YRV, the simulated 2-m temperatures are approximately 1 to 3°C lower than the surface air temperatures of CRU data in both the warm season (from June to September) and winter. Only for the late winter, the simulated NCN 2-m temperature is slightly lower than the observational data. So, the 2-m temperature of North China is reasonably well reproduced, compared to that of the other two regions.

In the lower troposphere, quite different from the South Asian monsoon area where the zonal circulation dominates, the EAM region has the same magnitude of the zonal and meridional winds. Therefore, the meridional wind is taken to represent the EAM strength (e.g., Ji et al., 1997). The annual cycles of meridional winds at the 1000-hPa level for the SEC, YRV, and NCN are given in Fig. 2b. For all three regions, the annual cycles of the meridional winds are well simulated, compared to the NCEP reanalysis. However, a stronger winter northerly and a weaker summer southerly are simulated over all three regions. Again, the simulated error of the annual cycle is lowest in North China, compared to that of the SEC and YRV.

The most important signal we pay attention to is, of course, the simulation of the East Asian precipitation. The model used here captures the coarse large-scale features of the seasonal evolution of the East Asian precipitation (Fig. 2c). For SEC, the seasonal evolution is well simulated, but the precipitation amounts in spring and summer are lower than the observed ones, mainly because the simulated WPSH shifts northward (eastward) in spring (summer) compared to that in the

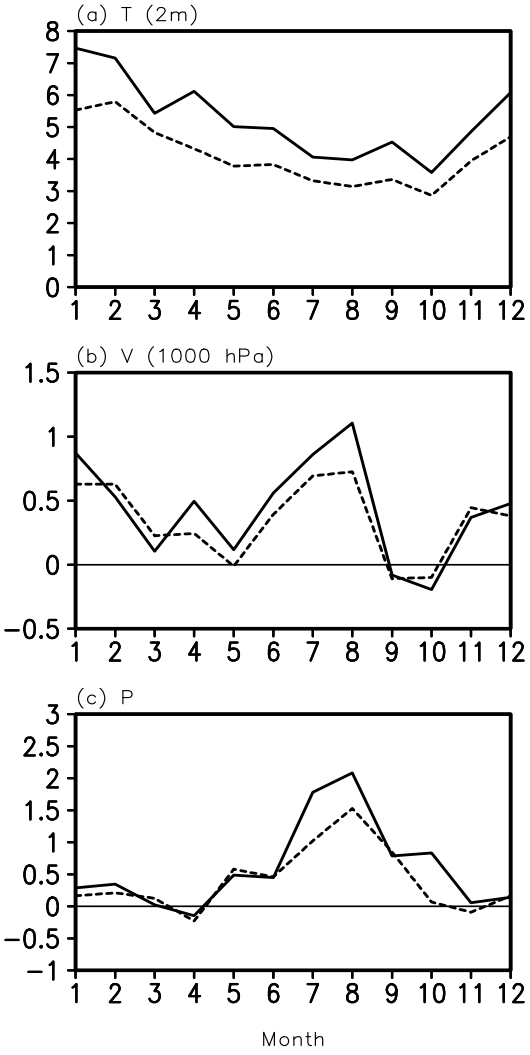

Fig. 4. The changes of annual cycles for the years 2071–2100 (relative to the present-day simulation) in North China (a) area mean 2-m temperatures (°C, land points only are considered), (b) area mean 1000-hPa meridional winds ($m\,s^{-1}$), and (c) area mean precipitations ($mm\,d^{-1}$, land points only are considered). The solid and dashed lines represent the IPCC SRES A2 and B2 scenarios, respectively.

NCEP reanalysis data (figure not shown). For the same reason, the YRV rainfall peak appears too early. For the NCN, the annual cycle of precipitation is quite well reproduced and the simulated summer rainfall peak is consistent with the observation.

As is clearly seen, the North China climate is reasonably well simulated by the coupled model, compared to that of the other two regions over East Asia. Our confidence for the exploration of its future change lies on this basis.

4. Change of the North China climate

In the following, for brevity, some words, such as "change" "increase" or "decrease", "strengthen" or "weaken", are used to represent the varied part of the simulated future climate relative to the simulated present-day one.

4.1 *Radiative forcing and sulfur emissions*

Figures 3a and 3b show radiative forcing and sulfur emissions for IPCC SRES A2 and B2 scenarios (Nakicenovic et al., 2000; IPCC, 2001). Until 2100, the total forcing of all greenhouse gases rises from the 1990 value of 2.0 $W\,m^{-2}$ to 8.1 $W\,m^{-2}$ for scenario A2 and 5.5 $W\,m^{-2}$ for scenario B2. The greenhouse gas concentrations in the old IS92a scenario (IPCC, 2001) are very similar to those in scenario A2. Larger differences between the two scenarios are found for the sulfur emissions. The global mean emission in scenario A2 is expected to increase by 50% until the 2030s and then decrease gradually, so that the emission of 2100 is approximately as large as present-day emissions. In scenario B2, a gradual decrease is assumed with the emissions in 2100 about 30% less than today's. Figure 3c shows the temporal evolution of the global mean temperature (2m) increase relative to the present-day mean value (from GSDIO experiment, 1961–1990). To depict the general trend, all values have been smoothed by a 5-year running mean. It is clearly seen that the trends generally follow the radiative forcing. The sulfate aerosol effect on the global mean temperature is also evident in Fig. 3c. Even though the increase of radiative forcing of all greenhouse gases in scenario A2 proceeds faster than in scenario B2 after 2020, the warming does not differ significantly from that in B2 until 2060, due to the enhanced sulfur emissions during this period. Until 2100, the global mean 2-m temperature increases 3.8°C in scenario A2 and 2.8°C in scenario B2.

It is also very interesting to note the differences between scenarios A2 and B2 before 2060. Before 2020, the sulfur emissions in scenario A2 are less than 100 $Tg\,S\,yr^{-1}$ and the greenhouse effect dominates for the global warming trend, since the simulated temperature increase is higher than in scenario B2. For scenario B2, the sulfur emissions decrease gradually and the radiative forcing of the greenhouse gases increases gradually. It is from 2020 to 2050 that the sulfur emission in scenario A2 reaches its large amount (more than 100 $Tg\,S\,yr^{-1}$) and the corresponding negative radiative forcing has a crucial effect, comparable to the positive radiative forcing of the greenhouse gases, on the warm-

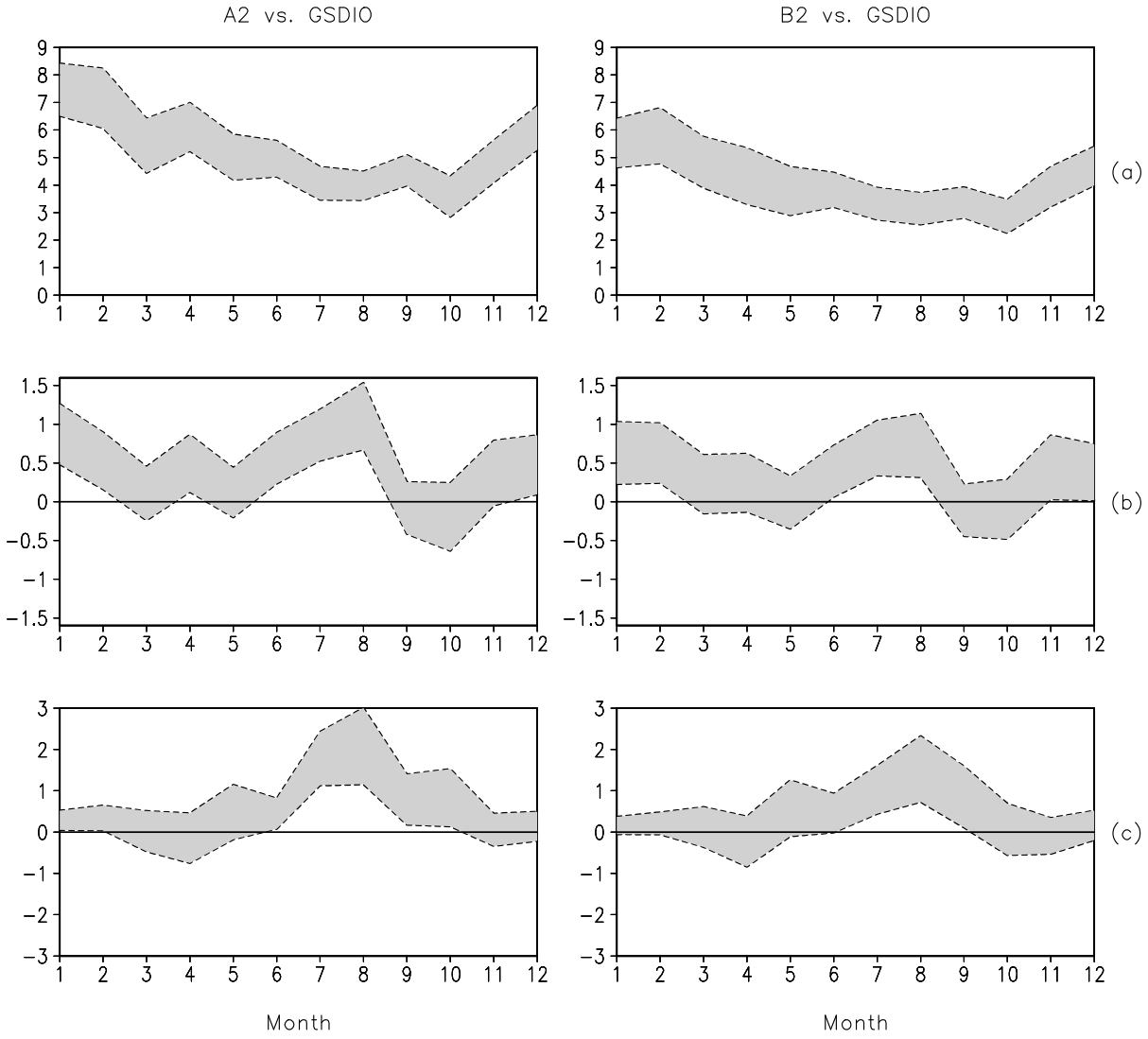

Fig. 5. The same as Fig. 4, but for the changes at the 95% confidence level. The left and right panels are for the changes in the IPCC SRES A2 and B2 scenarios relative to the present-day simulation, respectively.

ing trend. As a consequence, the temperature increase in scenario A2 from 2020 to 2050 is lower than that in scenario B2, and even not obvious from 2020 to 2040. This seems to suggest that the period of the warming observed in the past was the period of less sulfur emissions. In this paper, however, we selected the last three decades of the 21st century, for which the radiative forcing of the greenhouse gases dominate, to analyze the climate change of North China.

4.2 *Changes of annual and seasonal cycles*

Figure 4 gives the change of the temperature (2 m), 1000-hPa meridional velocity, and precipitation of North China in the last three decades of the 21st century, relative to their present-day values. Here we applied the optimal two-sided test for the significance of the change in question. The temperature increase varies in different months (Fig. 4a). Specifically, the temperature increase is higher in winter than in summer，implying that the temperature seasonality weakens slightly according to the definition of seasonality (Walsh and Lawler, 1981). In all months, the temperature changes are significant at the 95% confidence level (Fig. 5a). Due to the difference of radiative forcing, the annual mean temperature increase is approximately 1°C higher in scenario A2 (5.2°C) than in scenario B2 (4.2°C).

Figure 6 shows the temperature change distribution in all seasons. From the tropical ocean, via the SEC and YRV, to North China and its north side, the temperature increase becomes larger and larger. This

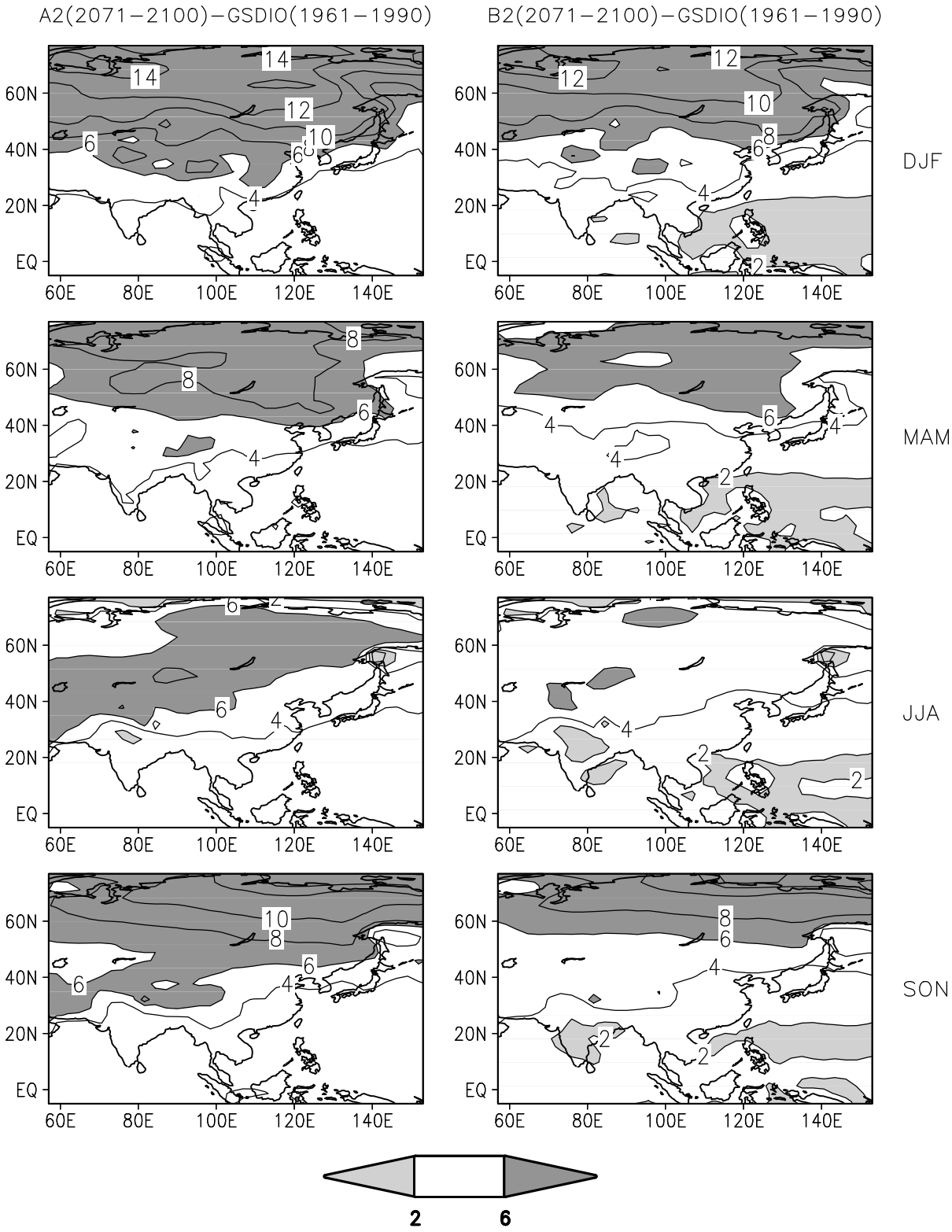

Fig. 6. The distributions of the mean 2-m temperature changes (°C) in winter (DJF), spring (MAM), summer (JJA), and autumn (SON) for the years 2071–2100. The left and right panels are for the IPCC SRES A2 and B2 scenarios, respectively.

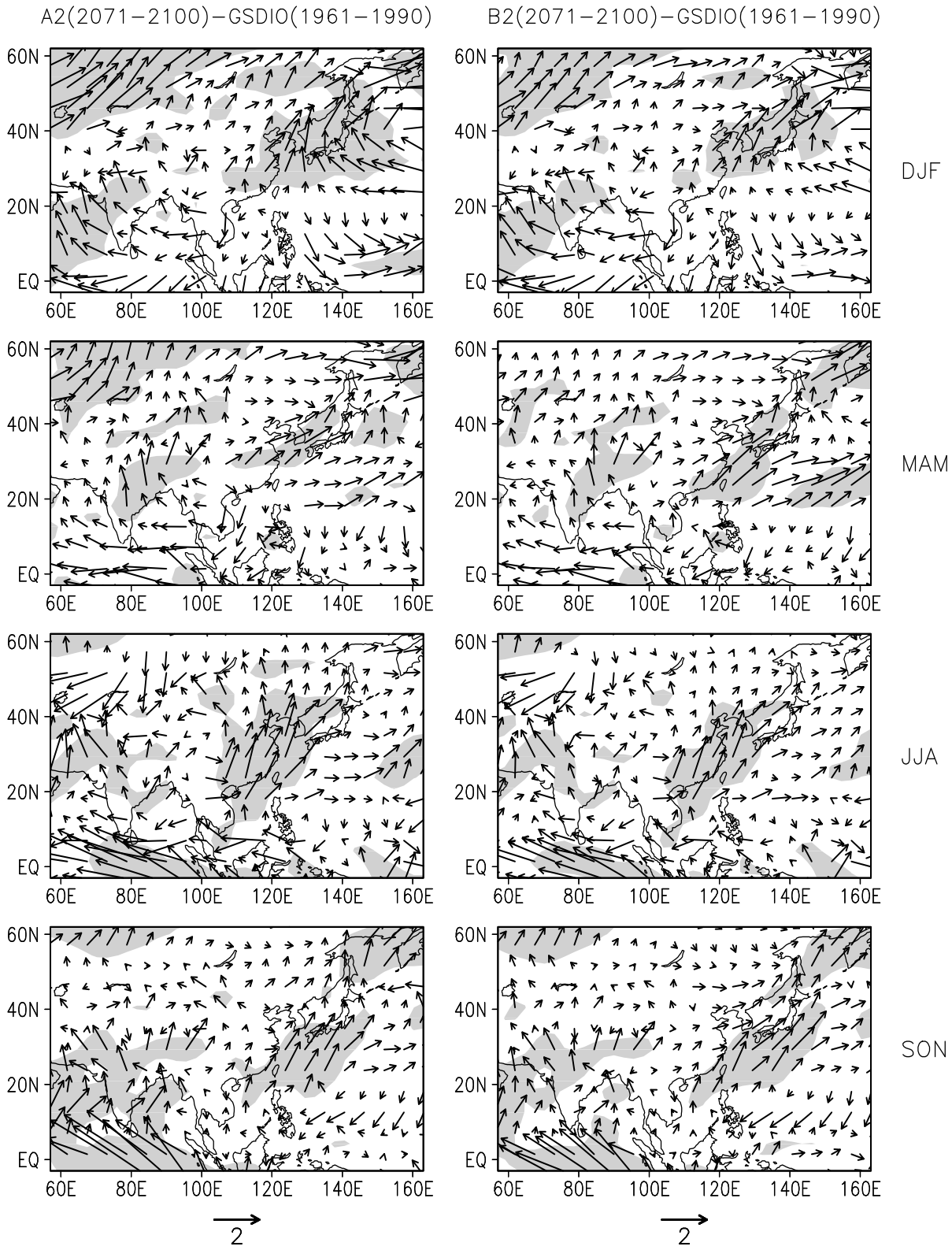

Fig. 7. The same as Fig. 6, but for the 1000-hPa wind ($m\,s^{-1}$). The shading marks the region where the southerly wind anomaly exceeds 0.5 $m\,s^{-1}$.

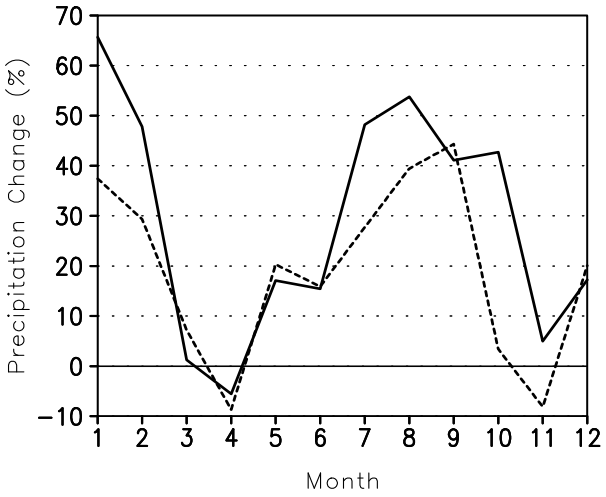

Fig. 8. The same as Fig. 4c, but in percentage.

is consistent with the consensus conclusion of many IPCC related studies that the warming in the higher latitude regions is larger than in the subtropics and the tropical ocean (IPCC, 2001). The inhomogeneous temperature increase in the EAM region and its adjacent oceans implies a change of the land-sea contrast, and hence a change of EAM circulation. In addition, the stronger temperature increase in scenario A2 than in scenario B2 is found not only over the mid and high latitude areas but also over the tropical oceans. The different radiative forcing is responsible for such a difference in the temperature change.

It is clearly seen in Fig. 4b that the 1000-hPa southerly wind strengthens in summer, whereas the northerly winter monsoon flow weakens. This implies the seasonality of the 1000-hPa meridional wind would not change significantly in the future. The change in meridional flow is in agreement with the surface warming distribution (Fig. 6). Meanwhile, the changes in meridional wind both in winter and summer are significant at the 95% level for the two scenarios (Fig. 5b). The changes in other seasons are not significant due to the considerably strong interannual fluctuation. The southerly wind anomaly in scenario A2 is stronger than in scenario B2. One can find from Fig. 7 that southerly wind anomalies dominate over East Asia and its adjacent sea in all seasons. But with careful inspection, only the summer and winter monsoon flows change significantly in both the A2 and B2 scenarios. In a coupled GCM simulation in which only greenhouse gases are taken into account, Hu et al. (2000) found a weakened Asian winter monsoon circulation. Our result with regard to the winter monsoon is consistent with this finding. As is well known, North China is affected directly by the East Asian monsoon. So the change of the land-sea thermal contrast not only causes the monsoon change but also leads to a change of the low-level wind of North China. It is noteworthy that the anomalous southerly wind converges in the area extending from the YRV to North China and the maximum convergence occurs in North China. This implies an increase of the moisture transport and convergence, hence, the precipitation.

It is very interesting to note that the simulated future precipitations over North China strengthen in summer and winter (Fig. 4c and Fig. 8) in both the A2 and B2 scenarios. The corresponding changes are significant at the 95% level in summer, while marginally significant in winter (Fig. 5c). Particularly in August, the precipitation increases 2.1 mm d^{-1} (54%) in scenario A2 and 1.5 mm d^{-1} (40%) in scenario B2. Quite surprisingly, the winter rainfall increase in percentage is comparable to its summertime increase (Fig. 8). In particular, the precipitation in January increases 65% in scenario A2 and 37% in scenario B2. The marginal significance of the change in winter, therefore, is influenced mainly by the strong interannual fluctuation (Fig. 10). The latter will be discussed in section 4.3. In addition, the seasonality of the rainfall is strengthened in the future, since the increase in summer is much larger than in the winter.

Figure 9 displays the distributions of the precipitation changes in all seasons. In winter, the apparent increase in the Asian continent lies in the high latitude region. Over North China the increase is somewhat small. In spring, the significant precipitation increase occurs to the northeastern side of the Bay of Bengal. Over North China and the East Asian monsoon area, little change is found. In summer, a strong precipitation increase is found from the YRV to North China and northeastern China. Particularly in North China, the strongest increase center is found there and its value exceeds 2.0 mm d^{-1} in scenario A2 and 1.5 mm d^{-1} in scenario B2. This is consistent with the change of the lower level wind anomalies as just discussed (Fig. 7). Another important feature is the anomalous precipitation increase over the Indian peninsula in both the A2 and B2 scenarios. This is caused by the enhancement of the Indian monsoon circulation in summer (Fig. 7). In autumn, the precipitation increases occur in North China. Especially in September, it meets significance at the 95% level. This implies that the future precipitation in September is tantamount to that of the present-day in June. The strong increase in autumn is also found over the Indian peninsula due to the strengthened (or prolonged) monsoon-like circulation (Fig. 7).

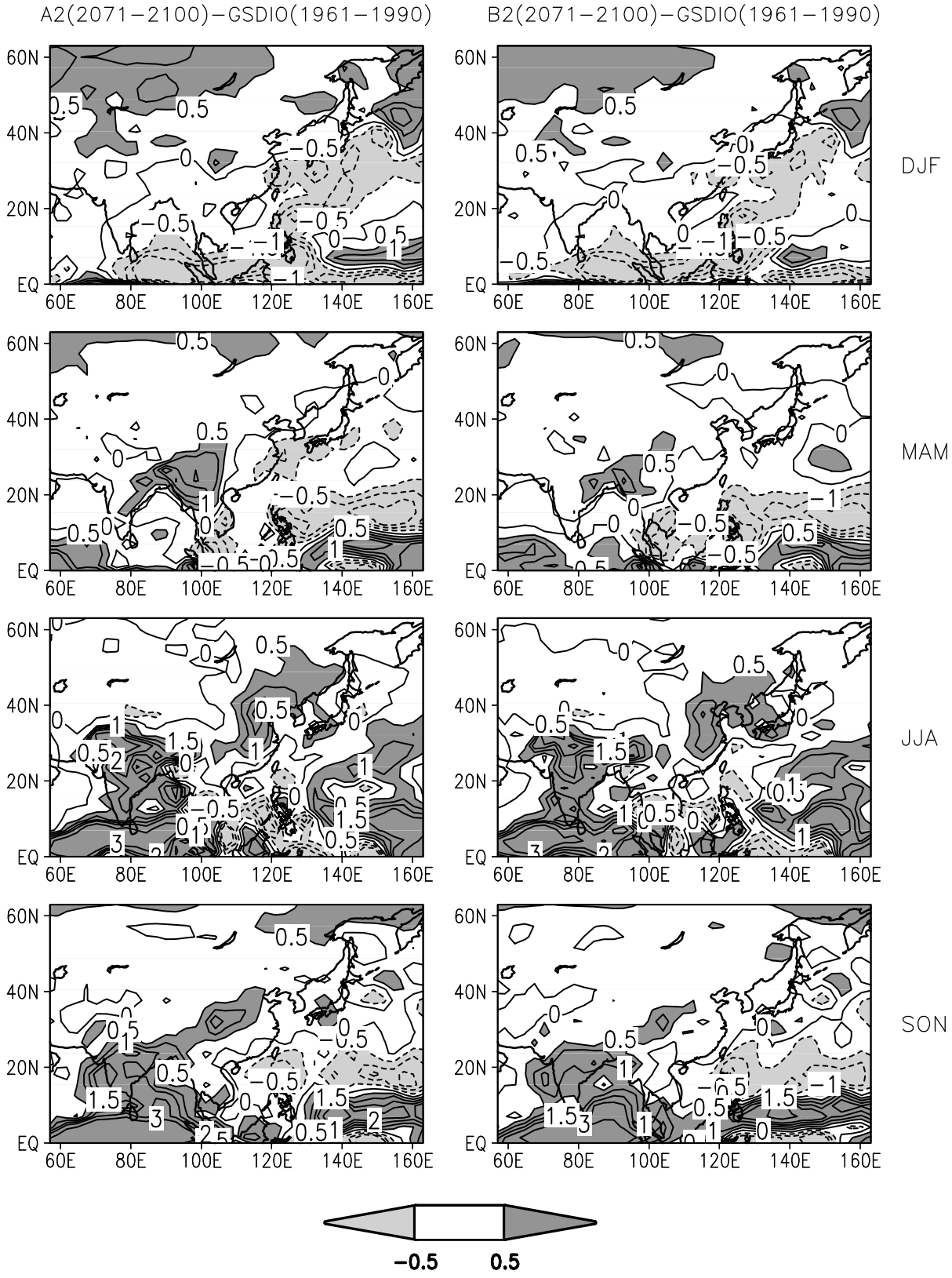

Fig. 9. The same as Fig. 6, but for the precipitation rate (mm d^{-1}).

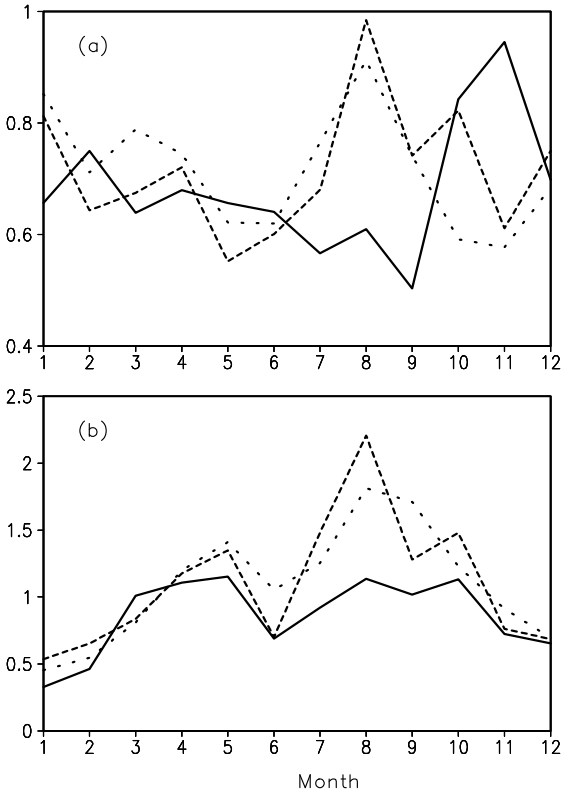

Fig. 10. Annual cycles of the standard deviations for (a) the 1000-hPa meridional wind ($m\,s^{-1}$) and (b) the precipitation ($mm\,d^{-1}$) in North China. The solid, dashed, and dotted lines are for the present-day climate simulation and the future climate simulations (2071–2100) with the IPCC SRES A2 and B2 scenarios, respectively.

4.3 *Change of interannual variation*

Apart from the mean climate change, the change of the interannual variability in the future climate is of social and economic importance as well, since it is closely related to the flood and drought disasters. Figure 10 shows the interannual variabilities of the 1000-hPa meridional wind and precipitation in North China for the present-day and future climate. For both the 1000-hPa meridional wind and precipitation, the interannual variability increases significantly in July, August, and September. This means that in the rainy season, North China would experience a larger rainfall variation (year to year) in the future than in the present-day and, hence meet a risk of flooding in the future (2071–2100). In contrast, the corresponding interannual variability change is not significant in the SEC and YRV (figure not shown).

5. Discussion and summary

An opinion has it that the summertime rainy area in East Asia would expand northward to North China after the mid 21st century. Our result in this work supports this idea. For North China, the summer (JJA) precipitation increase in the future (2071–2100) is about 136 mm in scenario A2 and 93 mm in scenario B2. So, we can calculate the total summer precipitation amounts of North China in the future in terms of the observed values (383 mm, from CRU data) and the increased amounts simulated. The total summer precipitation amounts for the last three decades of the 21st century are 476 mm in scenario B2 and 519 mm in scenario A2. As a consequence, they are comparable to the present-day summer precipitation amount of the YRV, i.e., 493 mm (from CRU data). Moreover, the YRV precipitation increases significantly in the future as well. According to this, North China would become a member of the East Asian rainy areas.

In this paper, we apply the newest emission scenarios of the sulfur and greenhouse gases, i.e., IPCC SRES A2 and B2 scenarios, to investigate the change of the North China climate with the ECHAM3/OPYC3 atmosphere-ocean coupled general circulation model. The main conclusion is as follows. In the last three decades of the 21st century, the global warming leads to the enhancement of the land-sea heat contrast, and as a consequence, to a strengthened (weakened) East Asian summer (winter) monsoon circulation. Due to the increased moisture transport and convergence, for which the change of the summer monsoon circulation is responsible, the summer precipitation increases significantly in North China. The rainfall seasonality increases as well in North China. It is suggested that the East Asian rainy area would expand northward to North China in the last three decades of the 21st century. In addition, the precipitation there would increase significantly in September. In July, August, and September, evident increases of the interannual variability of the precipitation are found for North China, implying a risk of floods in the future.

Acknowledgments. The first author would like to thank the Max-Planck-Institute for Meteorology for the support during his visit. The authors would like to thank two anonymous reviewers for their useful suggestions and comments on the manuscript. This work was jointly supported by the Key Project of the Chinese Academy of Sciences (KZCX2-SW-210), the Key Project of the Chinese Academy of Sciences (KZCX2-203), and the National Key Programme for Developing Basic Sciences (G1998040904). The first author is grateful to Profs. Wu Guoxiong and Huang Ronghui for their encouragement.

REFERENCES

Bacher, A., J. M. Oberhuber, and E. Roeckner, 1998: ENSO dynamics and seasonal cycle in the tropical Pa-

cific as simulated by the ECHAM4/OPYC3 coupled general circulation model. *Climate Dyn.,* **14**, 431–450.

Bueh Cholaw, and Ji Liren, 1999: Anomalous activity of East Asian winter monsoon and the tropical Pacific SSTA, *Chinese Science Bulletin*, **44**(10), 890–898.

Chang, C.-P., Y. Zhang, and T. Li, 2000: Interannual and interdecadal variations of East Asian summer monsoon and tropical Pacific SSTs. Part I: Roles of the subtropical ridge. *J. Climate*, **13**, 4310–4325.

Chen, Wen, and Hans-F. Graf, and Huang Ronghui, 2000: The interannual variability of East Asian winter monsoon and its relation to the summer monsoon. *Advances in Atmospheric Sciences*, **17**, 48–60.

Cubasch, U., and Coauthors, 2000: Simulation, Diagnosis and Detection of the Anthropogenic Climate Change (SIDDACLICH), Summery Report of the Project EU-Commission, Brussells, EUR 19310, ISBN 92-828-8864-9, 78pp.

Feichter, J., U. Lohmann, and I. Schult, 1997: The atmospheric sulfur cycle and its impact on the shortwave radiation. *Climate Dyn.*, **13**, 235–246.

Hu, Z.-Z., L. Bengtsson, and K. Arpe, 2000: Impact of global warming on the Asian winter monsoon in a coupled GCM. *J. Geophys. Res.*, **105**(D4), 4607–4624.

Hulme, M., Z. C. Zhao, and T. Jiang, 1994: Recent and future climate change in East Asia *Int. J. Climatol.*, **14**, 637–658.

IPCC, 2001: The Scientific Basis. Contribution of Working Group I to the Third Assessment Report of the Intergovernmental Panel on Climate Change (IPCC). *Climate Change 2001*, J. T. Houghton, Y. Ding, D. J. Griggs, M. Noguer, P. J. van der Linden and D. Xiao, Eds., Cambridge University Press, UK, 944pp.

Ji Liren, Sun Shuqing, K. Arpe, and L. Bengtsson, 1997: Model study on the interannual variability of Asian winter monsoon and its influence. *Advances in Atmospheric Sciences*, **14**, 1–22.

Kalnay, E., and Coauthors, 1996: The NCEP/NCAR 40-year reanalysis project. *Bull. Amer. Meteor. Soc.*, **77**, 437–471.

Lau, K.-M., 1992: East Asian winter monsoon rainfall variability and climate teleconnection. *J. Meteor. Soc. Japan*, **70**, 211–241.

Nakicenovic, N., and Coauthors, 2000: *IPCC Special Report on Emissions Scenarios*. Cambridge University Press, Cambridge, UK, 599pp.

New, M., M. Hulme, and P. D. Jones, 2000: Representing twentieth-century spacetime climate variability. Part II: Development of 1901–96 monthly grids of terrestrial surface climate. *J. Climate*, **13**, 2217–2238.

Nitta, Ts., and Z.-Z. Hu, 1996: Summer climate variability in China and its association with 500 hPa height and tropical convection. *J. Meteor. Soc. Japan*, **74**, 425–445.

Oberhuber, J. M., 1993: Simulation of the Atlantic circulation with a coupled sea-ice-mixed layer-isopycnal general circulation model. Part I: Model description. *J. Phys. Oceanogr.*, **22**, 808–829.

Roeckner, E., and Coauthors, 1996: The atmospheric general circulation model ECHAM-4: Model description and simulation of present-day climate. MPI-Report, No.218, 90pp.

Roeckner, E., L. Bengtsson, J. Feichter, J. Lelieveld, and H. Rodhe, 1999: Transient climate change simulations with a coupled atmosphere-ocean GCM including the tropospheric sulfur cycle. *J. Climate*, **12**, 3004–3032.

Roelofs, G.-J., and J. Lelieveld, 1995: Distribution and budget of O_3 in the troposphere calculated with a chemistry-general circulation model. *J. Geophys. Res*, **100**, 20983–20998.

Tao, S. Y., and L. X. Chen, 1987: A review of recent research on the East Asian monsoon in China. *Monsoon Meteorology*, Oxford University Press, Oxford, 60–92.

Walsh, P. D., and D. N. Lawler, 1981: Rainfall seasonality: Description, spatial patterns and change through time. *Weather*, **36**, 201–208.

Wang Shaowu, and Ye Duzheng, 1993: Analysis of the global warming during the last one hundred years. *Climate Variability*, Ye et al., Eds. China Meteorological Press, Beijing, 23–32.

Yasunari, T., 1991: The monsoon year: A new concept of the climatic year in the tropics. *Bull. Amer. Meteor. Soc.*, **72**, 1331–1338.